

# Measuring $CP$ nature of $h\tau\bar{\tau}$ coupling at $e^-p$ collider

Sukanta Dutta<sup>a,1</sup>, Ashok Goyal<sup>b,2</sup>, Mukesh Kumar<sup>c,3</sup>, Abhaya Kumar Swain<sup>d,1,2,3</sup>

<sup>1</sup>SGTB Khalsa College, University of Delhi (DU), Delhi, India.

<sup>2</sup>Department of Physics & Astrophysics, University of Delhi, Delhi, India.

<sup>3</sup>School of Physics and Institute for Collider Particle Physics, University of the Witwatersrand, Johannesburg, Wits 2050, South Africa.

**Abstract** The proposed future  $e^-p$  collider provides sufficient energies to produce the Standard Model Higgs Boson ( $h$ ) through  $W^\pm$  and  $Z$ -Boson fusion in charged and neutral current modes, respectively and to measure its properties. We take this opportunity to investigate the prospect of measuring the  $CP$  properties of  $h$  through  $h \rightarrow \tau^+\tau^-$ , where  $\tau^-$  ( $\tau^+$ ) decays to a charged pion  $\pi^-$  ( $\pi^+$ ) and a neutral pion  $\pi^0$  in association with neutrino (anti-neutrino). An interesting  $CP$  sensitive angular observable  $\alpha_{CP}$  between the two  $\tau$ -leptons decay plane in the  $\pi^+\pi^-$  centre of mass frame is proposed and investigated in this work. For fixed electron energy of 150 GeV along with 7 (50) TeV of proton energy, the  $CP$  phase can be measured approximately to  $25^\circ$  ( $14^\circ$ ) at integrated luminosity of  $1 \text{ ab}^{-1}$  for  $-80\%$  polarised electron at 95% confidence level.

## 1 Introduction

After the Higgs Boson ( $h$ ) discovery at the Large Hadron Collider (LHC) [1–4], measurement of its properties and their possible deviation from the Standard Model (SM) predictions are important to explore physics beyond the SM (BSM) [5]. In this context the proposed Large Hadron electron Collider (LHeC) [6–9] with centre of mass (CM) energy  $\sqrt{s} \approx 1.3 \text{ TeV}$  with possible enhancement to 3.5 TeV at the proposed Future Circular Electron Hadron Collider (FCC-eh) programme at CERN may act as potential Higgs factories offering enormous scope to study the Higgs Boson properties [10–12]. Exploring  $CP$  nature of the  $h$  coupling to the SM particles as occurs in several extensions of the SM through the interaction of multiple Higgs-sector, in supersymmetric theories and so on, has become important since

$CP$  violation in the Higgs Boson sector would impact baryogenesis in the early Universe [13–17].

The ATLAS and CMS collaborations have probed the  $CP$  nature of the  $h$  coupling and have excluded the pure  $CP$  odd nature at 99% confidence level (C.L.) [18–21], and this leaves the possibility of  $h$  either being an admixture of  $CP$ -even and  $CP$ -odd states or a pure  $CP$ -even state. Current bounds on the mixing angle are weak, and large mixing is not ruled out. This property has been analysed in a clean di-lepton pair production through  $h \rightarrow ZZ^* \rightarrow 4\ell$  [22–25]. However, this process has low sensitivity to determine the  $CP$  violating phase because of the dominant  $CP$  even  $hZZ$  coupling. The  $CP$ -odd scalar coupling to  $Z/W^\pm$  vector Bosons can arise only from the dimension six SM gauge invariant operators and are likely to be subdominant as compared to the  $CP$ -even SM couplings. Since the Yukawa coupling of  $h$  to the third generation fermions is larger, it is natural to expect that studying  $CP$  properties with them might play an important role. In Ref. [12], authors studied the  $h$  coupling with top-quark in the LHeC environment.

It is also important to mention that the choice of  $CP$ -odd observable are often sensitive to the production mechanism of Higgs Boson. The dominant gluon fusion channel at the LHC suffers from alarmingly large SM background [26, 27] which, in turn, reduce the signal rate. In contrast,  $h$  production through vector-Boson fusion (VBF) has clear advantage over the gluon-fusion mode. The VBF leads to distinctive topology resulting in an enhancement of the signal to background ratio [28].

In the context of measuring  $CP$  characteristics of Higgs Boson through the  $\tau$ -lepton Yukawa coupling, several angular observables has been proposed in the literature at the collider experiments in Refs. [22, 26, 27, 29–61]. These observables are defined in the  $\tau$ -lepton pair centre of mass frame. However, reconstructing the CM frame of  $h$  in  $\tau^+\tau^-$  channel is extremely challenging. Firstly, because of the un-

<sup>a</sup>e-mail: Sukanta.Dutta@gmail.com

<sup>b</sup>e-mail: agoyal45@yahoo.com

<sup>c</sup>e-mail: mukesh.kumar@cern.ch

<sup>d</sup>e-mail: abhaya.kumar.swain@cern.ch

known CM energy of collision between the incoming partons in hadron colliders and secondly, the presence of the neutrinos which escape the detector leaving the transverse momentum imbalance to infer their presence. Since there are multiple neutrinos present in the final state, it is very difficult to reconstruct the  $\tau^\pm$  momenta. However, it is well known that the  $\tau$ -lepton has finite decay length which results in a measurable impact parameter. This additional measurement not only improve the  $\tau^\pm$  momentum reconstruction [60, 62] but also leads to construct the  $CP$  sensitive angular observables [61, 63] without even requiring the reconstruction of CM frame of  $h$ . One such angular observable has been explored to measure the  $CP$  phase of the  $\tau$ -lepton Yukawa coupling at the CMS collaboration [64]. This measurement constraint the  $CP$  phase to  $4^\circ \pm 17^\circ$  ( $\pm 36^\circ$ ) at 68% (95%) C.L. with CM energy of 13 TeV at integrated luminosity,  $\mathcal{L} = 137 \text{ fb}^{-1}$ .

In this article we focus on  $h$  production at the proposed future  $e^-p$  colliders, namely, the LHeC and FCC-eh and will probe the  $CP$  nature of the  $h\tau\bar{\tau}$  coupling in this environment. We will discuss the involved challenges in the analysis and probe one of the observable as mentioned above. The Higgs Boson is produced through the charged current (CC)  $W^+W^-$  fusion and the neutral current (NC)  $ZZ$  fusion giving rise to a forward jet and missing energy in the former and a forward jet with scattered electron in the latter as shown in Fig. 2 with  $h$  decaying to  $\tau^+\tau^-$  pair. Further we choose  $\tau^\pm$  decay to  $\rho^\pm$  with corresponding  $\nu_\tau$  and  $\rho^\pm$  decays to  $\pi^\pm\pi^0$  with approximately 100% probability. We have picked up this channel among all other  $\tau^\pm$  decay channels because of the larger branching ratio of 25.9% to demonstrate the prospect of measuring the  $CP$  phase of the  $h\tau\bar{\tau}$  coupling. In this study we only modify the  $h\tau\bar{\tau}$  vertex by assuming other involved couplings to be the SM one.

In section 2 we discuss the Lagrangian which is used to parameterize the  $CP$  phase dependent vertex of the  $h\tau\bar{\tau}$ . Then we describe the simulation that we follow to perform the analysis. Next in section 3 we elucidate the observable that is employed to constrain the  $CP$  admixture of the  $h\tau\bar{\tau}$  coupling. In the following section 4, we illustrate the results and section 5 is devoted for summary and discussions of our analysis.

## 2 Formalism & Simulation

In this analysis we assume the measured Higgs Boson mass at  $m_h = 125 \text{ GeV}$  to be a mixture of  $CP$  even and odd scalar and the interaction between  $h$  and  $\tau^\pm$  is given by

$$\mathcal{L}_{h\tau\bar{\tau}} = -\left(\sqrt{2}G_F\right)^{1/2} m_\tau \bar{\tau}(\tilde{a} + i\tilde{b}\gamma_5)\tau h; (\tilde{a} > 0) \quad (1)$$

where  $G_F$  is the Fermi constant,  $m_\tau$  is the mass of  $\tau$ -leptons and the parameters  $\tilde{a}$  ( $\tilde{b}$ ) are dimensionless couplings for

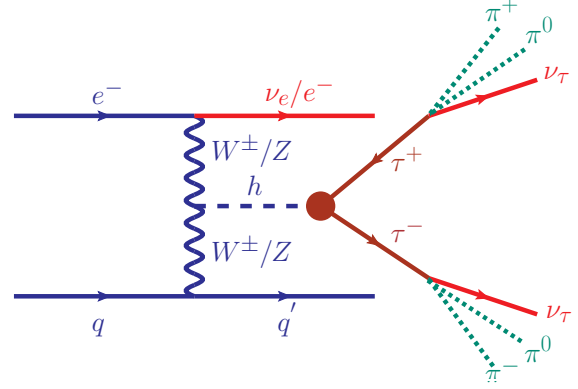


**Fig. 1** Leading order Feynman diagram for  $h$  production via the charged / neutral current process in  $e^-p$  collider. The figure shows the process  $e^-p \rightarrow \nu_e/e^- h j$ ,  $h \rightarrow \tau^+\tau^-$  with  $\tau^\pm \rightarrow \pi^\pm\pi^0\nu_\tau$ ,  $q$  are the partons from proton and  $q'$  is the scattered jets.

the  $CP$  even (odd) part of the Lagrangian. In, an alternative parametrization, the Lagrangian in equation (1) can be expressed as

$$\mathcal{L}_{h\tau\bar{\tau}} = -C_{\text{eff}}^\tau \bar{\tau}(\cos\phi_\tau + i\sin\phi_\tau\gamma_5)\tau h, \quad (2)$$

where the  $C_{\text{eff}}^\tau \equiv \left(\sqrt{2}G_F\right)^{1/2} m_\tau \sqrt{\tilde{a}^2 + \tilde{b}^2}$  is the effective coupling and  $\phi_\tau \equiv -\pi/2 \leq \tan^{-1}(\tilde{b}/\tilde{a}) \leq \pi/2$  is the mixing angle of the scalar and pseudo-scalar component of the couplings with leptons. The choices  $(\tilde{a} = 1, \tilde{b} = 0)$ ,  $(\tilde{a} = 1/\sqrt{2}, \tilde{b} = 1/\sqrt{2})$  and  $(\tilde{a} = 0, \tilde{b} = 1)$  correspond to SM pure  $CP$ -even ( $\phi_\tau = 0^\circ$ ), a 50% mixed ( $\phi_\tau = 45^\circ$ ) and pure  $CP$ -odd pseudo-scalar ( $\phi_\tau = 90^\circ$ ) states for both the parametrization respectively. Also, they satisfy  $\sqrt{\tilde{a}^2 + \tilde{b}^2} = 1$  implying that the effective strength of the Yukawa couplings  $C_{\text{eff}}^\tau$  for the mixed or pure states are identical to that of SM modulo the dependence on mixing angle. It is to be noted that the mixing angle  $\phi_\tau$  is specific for the  $\tau$  lepton and is not universal with respect to (*w.r.t.*) other SM fermions. In our analysis, we have assumed all other couplings of the fermions and gauge Bosons with the scalar  $h$  to be identical to those of SM.

As mentioned in the introduction, we consider the following  $\tau^\pm$  decay mode in our analysis:  $\tau^{-(+)} \rightarrow \nu_\tau(\bar{\nu}_\tau) + \rho^{-(+)} \rightarrow \nu_\tau(\bar{\nu}_\tau) + \pi^{-(+)} + \pi^0$ . The effective Lagrangian describing the  $\rho^\pm$  decay mode is given as

$$\mathcal{L}_{\pi^\pm, \pi^0} = \sqrt{2}G_F f_2 \bar{\tau}\gamma^\mu P_L \nu_\tau (\pi^- \partial_\mu \pi^- - \pi^- \partial_\mu \pi^0) + \text{h.c.} \quad (3)$$

with  $f_2 = \sqrt{2} \cos\theta_C F_\rho(Q^2)$ .

The detailed discussions on parametrization of the form factor  $F_\rho(Q^2)$  are found in references [65–67].

We have implemented the Lagrangians given in equations (1) and (3) in FeynRules [68] to build the model file and simulated the parton level events using MadGraph5 [69] with NN23L01 [70] parton distribution function. The factorisation and renormalisation scales for the simulation are

Process	LHeC : $\sigma(\text{fb})$	FCC-eh : $\sigma(\text{fb})$
Signal: CC	0.56 (1.0)	1.72 (3.11)
Signal: NC	0.1 (0.11)	0.37 (0.41)

**Table 1** SM cross sections for the CC and NC processes as shown in Fig. 1 for unpolarised (–80% polarised) 150 GeV electron beam colliding with 7 TeV and 50 TeV proton beams corresponding to LHeC and FCC-eh respectively.

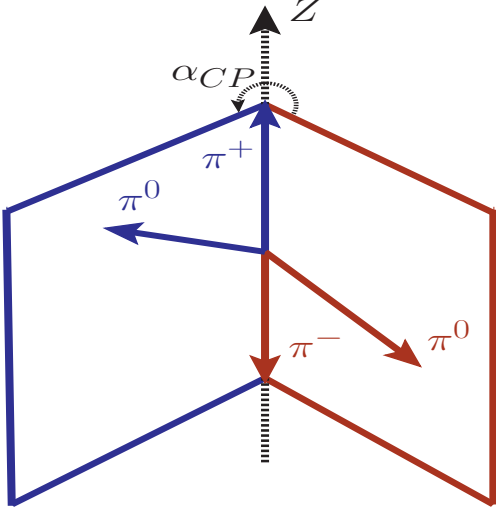


**Fig. 2** Representative diagram for the decay planes spanned by the charged and neutral pion produced from respective  $\tau^\pm$ -lepton in the  $\pi^+\pi^-$  rest frame. The angle between the two decay planes is denoted as  $\alpha_{CP}$  which is utilised here to explore the  $CP$  admixture of the  $h\tau\bar{\tau}$  coupling.

taken to be the default MadGraph5 dynamic scales. Both the CC and NC channels are simulated in the LHeC set up with electron (proton) beam energy to be 150 (7000) GeV and FCC-eh set up with proton beam energy of 50 TeV keeping other parameters unchanged. The analysis is performed for the unpolarised and –80% polarised electron beams, respectively. In addition, we require transverse momenta of charged pions  $p_{T\pi^\pm} \geq 20$  GeV.

In Table 1, the simulated CC and NC cross-sections are shown for 150 GeV unpolarised and –80% polarised electron beam colliding with 7 (50) TeV proton beam corresponding to the proposed LHeC (FCC-eh) collider. Further, we discuss the  $CP$  sensitivity of  $h\tau\bar{\tau}$  coupling in the next section.

Before, concluding this section, we briefly mention the potential backgrounds to CC and NC processes. The dominant SM tree level background for the CC process comes from  $W^+W^-$  fusion process  $e^-p \rightarrow \nu_e j Z/Z^*/\gamma^*$ , while backgrounds for NC process are induced by the  $\gamma^*Z\gamma$ ,  $Z^*Z\gamma$ ,  $\gamma^*ZZ$  and  $Z^*ZZ$  vertices either at the one loop level or through the higher dimensional model independent effective operators. The  $\tau^-\tau^+$  pair emanating from the neutral on-shell/

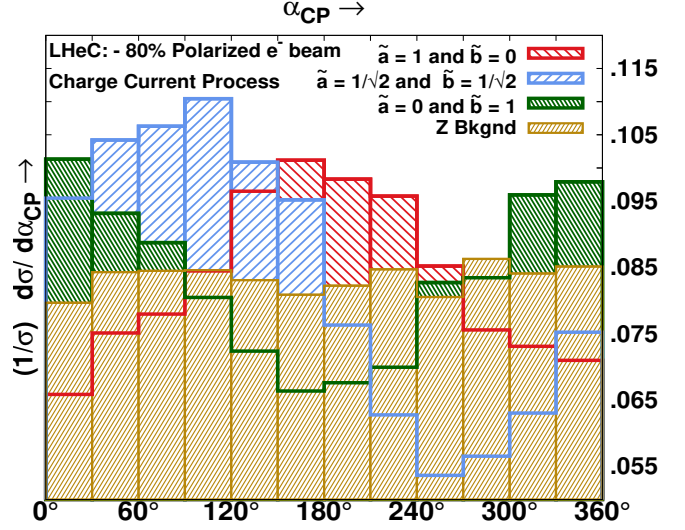


**Fig. 3** Normalized differential cross-sections w.r.t.  $CP$  sensitive observable  $\alpha_{CP}$  for the process  $e^-p \rightarrow (h \rightarrow \tau^+\tau^-) \nu_e \text{jets}$ ; and  $\tau^{-(+)} \rightarrow \nu_\tau (\bar{\nu}_\tau) + \rho^{-(+)} \rightarrow \nu_\tau (\bar{\nu}_\tau) + \pi^{-(+)} + \pi^0$  corresponding to SM pure  $CP$ -even (in red), 50% mixed (in blue) and pure  $CP$ -odd (in green) states respectively. The contribution from dominant  $Z$  background channel is shown in golden yellow. These distributions are simulated for LHeC set up with –80% polarised 150 GeV electron and unpolarised 7 TeV proton beams.

off-shell gauge Bosons decay poses a different angular distribution when compared with those produced from the decay of the mixture of scalar and pseudo-scalar. This has a bearing on the angular distribution on the decay products  $\tau^\pm$  in  $\rho^\pm$  mode and can be suppressed with appropriate selection cuts. The contribution from the dominant on-shell  $Z$ -decay can be vetoed by imposing a selection cut on the invariant mass of the  $\tau^-\tau^+$  pairs.

### 3 $CP$ -odd Observable

In this section we discuss the observable that are well suited to explore the  $CP$  nature of the  $h\tau\bar{\tau}$  coupling at the LHeC and FCC-eh. As discussed in Introduction, the major challenge comes from the neutrinos produced from decay of  $\tau$ -leptons and/ or the additional neutrino in the forward direction produced in association with the Higgs Boson for the charged current. These neutrinos escape detection and their presence can only be deduced from the momentum imbalance which engender measurement of the large missing transverse momenta.

There are various methods exist in the literature [71–78] to reconstruct the  $\tau$ -lepton momentum to construct  $CP$  sensitive observables at the LHC. However, in the present analysis at the LHeC/ FCC-eh the presence of additional neutrino in the charged current process makes it extremely challenging to reconstruct the  $\tau^\pm$  momenta. Therefore, we do not attempt any reconstruction of  $\tau^\pm$  momenta instead

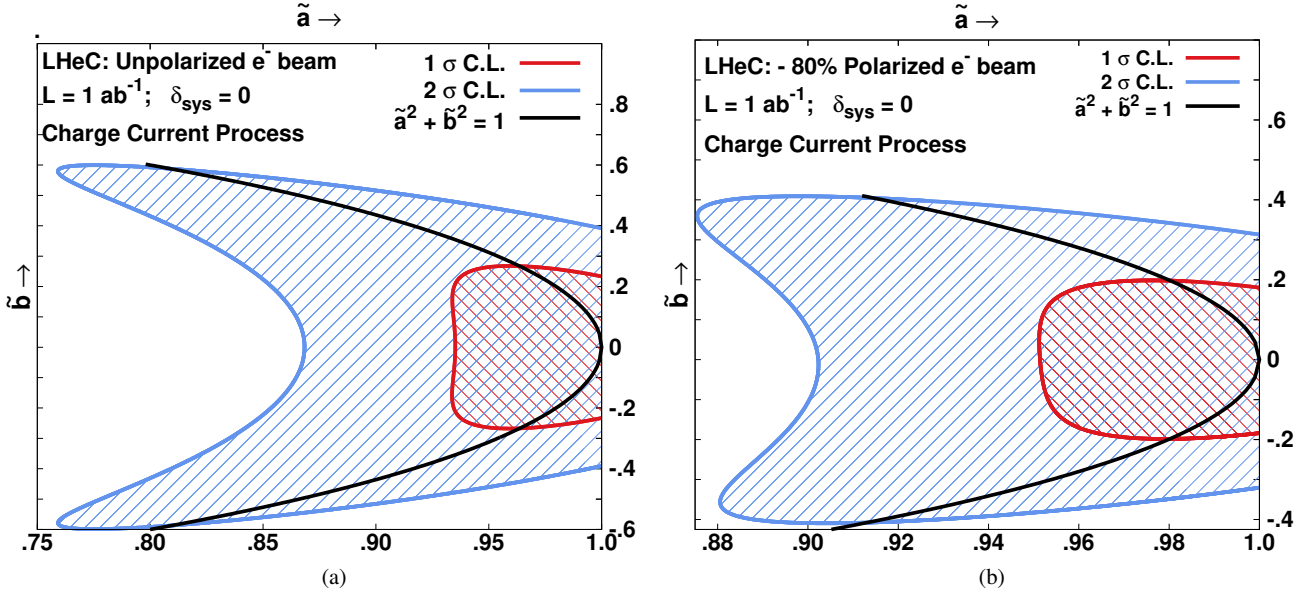


**Fig. 4** 68% (in red) and 95% (in blue) C.L. exclusion contours are drawn in  $\tilde{a} - \tilde{b}$  plane using differential bin-width  $\Delta\alpha_{CP} = 30^\circ$ . In each panel the intersecting points of the black contour with the one and two sigma contours depict the respective mixing angles  $\phi_\tau$  with SM like Yukawa coupling strength. Shaded interiors of the respective contours are however remain insensitive to the collider.

utilise the charged and neutral pion's momenta to compute a  $CP$  sensitive observable in the charged pion's CM frame [61].

To scrutinise the nature of the  $\tau$ -lepton Yukawa coupling, we simulate the  $\tau^+ - \tau^-$  events corresponding CC and NC processes and allow them to decay in  $\rho^\pm$  mode for LHeC and FCC-eh in MadGraph5. Our method is based on analysing the acoplanarity angle of the two planes, spanned by  $\rho^+$  and  $\rho^-$  decay products respectively and defined in  $\pi^+ - \pi^-$  rest frame known as Zero Momentum Frame (ZMF) as displayed in Fig. 2. Accordingly, on boosting the momentum of the simulated charged and neutral pions in ZMF of charged pions  $\pi^+$  and  $\pi^-$ ,  $CP$  sensitive observable is defined as

$$\alpha'_{CP} \equiv \arccos(\hat{p}_{0\perp}^+ \cdot \hat{p}_{0\perp}^-) \times \text{sgn}(\hat{p}_{\pi^-} \cdot (\hat{p}_{0\perp}^+ \times \hat{p}_{0\perp}^-)), \quad (4)$$

where the unit three momentum vectors  $\hat{p}_{\pi^\pm}$  specify the directions of the charged pions in ZMF and  $\hat{p}_{0\perp}^\pm$  ( $\hat{p}_{0\perp}^\pm$ ) is the unit transverse component of the three momentum for neutral pion *w.r.t.* the direction of accompanying charged pion  $\pi^-$  ( $\pi^+$ ) in ZMF. From equation (4) it follows that  $0^\circ \leq \alpha'_{CP} \leq 360^\circ$ .

The nature of the Yukawa coupling is hidden in the correlations among the spin vectors  $s^-$  and  $s^+$  corresponding to  $\tau^-$  and  $\tau^+$  in their respective rest frames for which the partial decay width of  $h$  is expressed as

$$\Gamma(h \rightarrow \tau^+ \tau^-) \propto 1 - s_{\parallel}^- s_{\parallel}^+ \pm C s_{\perp}^- s_{\perp}^+, \quad (5)$$

where  $C$  is complex and unitary. The correlation term for the transverse component in equation (5) is real and positive

(negative) for pure  $CP$  even (odd) state but complex for a mixed state. The parity information of  $h$  is further encoded in correlations among the decay products of the  $\tau$ s confined in the planes  $\perp$  to  $\tau^+$  and  $\tau^-$  axes. However, the destructive interference among the three polarised states of the intermediate particle  $\rho^\pm$  smear the sensitivity of  $\alpha'_{CP}$  in equation (4) due to the modified correlation term for transverse component of spin vectors in equation (5). Therefore, to unfold the information of a mixed state we further impose a selection cut (filter) and divide the simulated  $\tau$  decay events into two regions, depending on the sign of  $Y_{\tau^-\tau^+}$  [44, 57, 64]:

$$Y_{\tau^-\tau^+} = (Y_{\tau^-} - Y_{\tau^+}) = \left[ \frac{E_{\pi^-} - E_{\pi_{\tau^-}^0}}{E_{\pi^-} + E_{\pi_{\tau^-}^0}} \right] \times \left[ \frac{E_{\pi^+} - E_{\pi_{\tau^+}^0}}{E_{\pi^+} + E_{\pi_{\tau^+}^0}} \right] \quad (6)$$

where  $E_{\pi^\pm}$  and  $E_{\pi^0}$  are the energies of charged and neutral pions in the respective  $\tau^\pm$  rest frames. Taking into account the impact of sign of  $Y_{\tau^-\tau^+}$  we re-define the observable  $\alpha'_{CP}$  as

$$\alpha_{CP} = \begin{cases} \alpha'_{CP}, & \text{for } Y_{\tau^-\tau^+} \geq 0 \\ 360^\circ - \alpha'_{CP}, & \text{for } Y_{\tau^-\tau^+} < 0. \end{cases} \quad (7)$$

We study and analyse the differential distribution of cross-sections *w.r.t.*  $CP$  sensitive observable  $\alpha_{CP}$  for the available kinetic phase space corresponding to varying mixing angle  $-\pi/2 \leq \phi_\tau \leq \pi/2$ . It is observed that due to adoption of a common decay procedure for  $h$  decay to a pair of  $\tau^\pm$  and further  $\tau^\pm$  decaying in  $\rho^\pm$  mode in simulating CC and NC processes, the shape profile of the normalized differential distributions  $(1/\sigma)(d\sigma/d\alpha_{CP})$  are found to be similar. The shape profile of normalized distributions for LHeC and FCC-eh

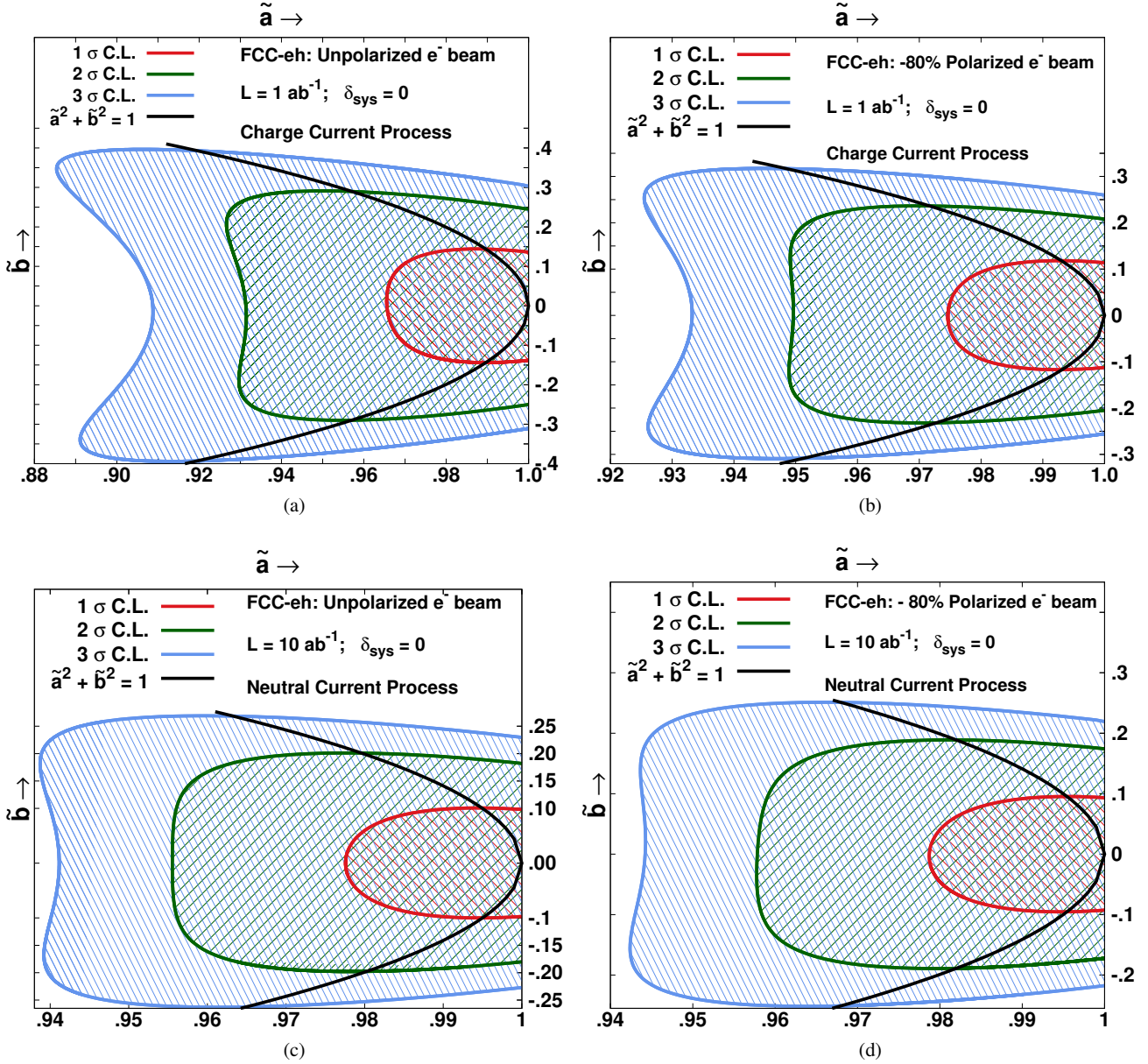


**Fig. 5** 68% (in red), 95% (in green) and 99.7% (in blue) C.L. exclusion contours are drawn in  $\tilde{a} - \tilde{b}$  plane using differential bin-width  $\Delta\alpha_{CP} = 30^\circ$ . In each panel the intersecting points of the black contour with the one, two and three  $\sigma$  contours depict the respective mixing angles  $\phi_\tau$  with SM like Yukawa coupling strength. Shaded interiors of the respective contours are however remain insensitive to the collider.

operating at two different CM energy are also found to be same as the  $\alpha_{CP}$  in ZMF is designed to be responsive only to the mixing angle  $\phi_\tau$ . For an illustration, in Fig. 3 we display the normalized differential cross-sections for CC process corresponding to three set of parameters discussed in section 2 for a 150 GeV –80% polarised electron beam colliding with a 7 TeV unpolarised proton beam at LHeC setup. The red, green and blue shaded histograms in Fig. 3 corresponds to three choices of parameter sets:  $(\tilde{a} = 1, \tilde{b} = 0)$ ,  $(\tilde{a} = 1/\sqrt{2}, \tilde{b} = 1/\sqrt{2})$  and  $(\tilde{a} = 0, \tilde{b} = 1)$  respectively.

The  $\alpha_{CP}$  differential distributions are also studied for dominant irreducible backgrounds in CC and NC channels, where  $Z/\gamma^*$  produced through gauge Boson fusion decays to a pair of  $\tau^\pm$  which then further decay to pions and neutrino/anti-neutrino in  $\rho^\pm$  mode. In Fig. 3 the flat golden yellow histogram depicts the contribution from  $Z$  background implying that the constructed  $CP$  observable is insensitive to the  $\tau^\pm$  decays.



#### 4 Results and Discussions

In order to estimate the sensitivity of the observable  $\alpha_{CP}$  to constrain the  $CP$  mixing angle of the  $h\tau\bar{\tau}$  coupling we have defined  $\chi^2$  as,

$$\chi^2(\tilde{a}, \tilde{b}) = \sum_{k=1}^n \left( \frac{N_k^{\phi_{\tau}=0} - N_k^{\phi_{\tau} \neq 0}}{\delta N_k^{\phi_{\tau}=0}} \right)^2; \quad (\tilde{a} > 0), \quad (8)$$

where

$$\delta N_k^{\phi_{\tau}=0} = \sqrt{N_k^{\phi_{\tau}=0} (1 + \delta_{sys}^2 N_k^{\phi_{\tau}=0})}. \quad (9)$$

Here  $k^{\text{th}}$  bin events  $N_k^{\phi_{\tau}=0} \equiv N_k^{\phi_{\tau}=0}(\tilde{a}=1, \tilde{b}=0)$  and  $N_k^{\phi_{\tau} \neq 0} \equiv N_k^{\phi_{\tau} \neq 0}(\tilde{a} \neq 0, \tilde{b} \neq 0)$  are the number of pure  $CP$ -even state (SM prediction) and  $CP$ -mixed state events respectively for a given integrated luminosity  $\mathcal{L}$ . The  $\delta_{sys}$  is an approximate systematic error which includes the luminosity uncertainty.

Assuming that the deviations in the number of events from the SM predicted pure  $CP$ -even state are due to variation of either the strength of the coupling or the mixing angle  $\phi_{\tau} \neq 0$ , we perform the  $\chi^2$  analysis with the histograms drawn from the parton level one dimensional differential cross-sections *w.r.t.*  $\alpha_{CP}$  by varying  $\tilde{a}$  and  $\tilde{b}$ . Using the differential bin-width  $\Delta\alpha_{CP} = 30^\circ$ , the  $\chi^2$  is computed for one degree of freedom in the two-dimensional plane spanned by  $\tilde{a} - \tilde{b}$ .

The one  $\sigma$  (in red) and two  $\sigma$  (in blue) exclusion contours in  $\tilde{a} - \tilde{b}$  plane are depicted in Fig. 4 for the charge current process at LHeC with 150 GeV electron beam and 7 TeV proton beam with zero systematic error and an integrated luminosity of  $\mathcal{L} = 1 \text{ ab}^{-1}$ . The left and right panels in Fig. 4 correspond to the unpolarised and  $-80\%$  polarised electron beams respectively. The unshaded exterior regions corresponding to respective contours can be probed by the proposed LHeC collider. Restricting the magnitude of the coupling to be SM like, we draw a contour  $\sqrt{\tilde{a}^2 + \tilde{b}^2} = 1$  depicted in black which intersect the three  $\chi^2$  contours. The two intersecting coordinates define the respective lower limits of the mixing angle  $\tan^{-1}(\tilde{b}/\tilde{a})$  that can be measured in the proposed collider at 68% and 95% C.L. respectively. These limits on the mixing angles for the unpolarised and  $-80\%$  polarised electron beams are given in Table 2. The  $\chi^2$  analysis are also performed with non-zero systematic errors for  $\delta_{sys}$  of the order of 5% and 10% respectively with the same differential distributions and the corresponding relaxed lower limits of the mixing angle are given in Table 2 at 1  $\sigma$ , 2  $\sigma$  and 3  $\sigma$  C.L. respectively.

The  $\chi^2$  analysis for  $\alpha_{CP}$  distributions from NC process are also performed with unpolarised and polarised beams respectively but the corresponding sensitivity limits on the mixing angle are found to be rather weak due to comparatively small cross-sections as shown in the Table 1.

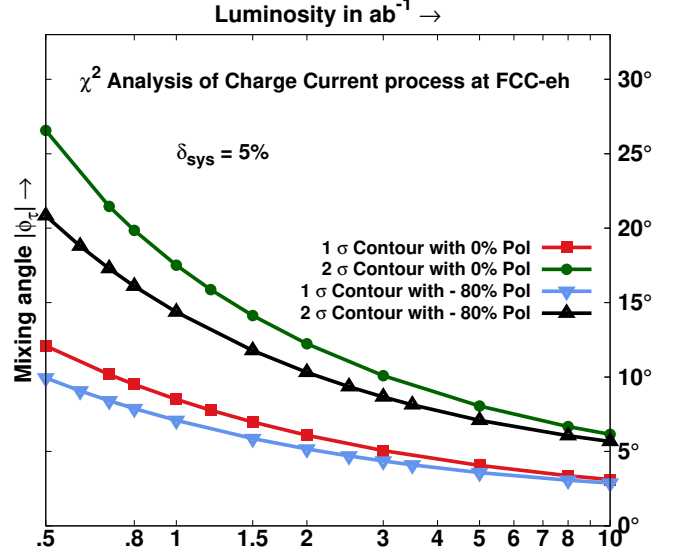


**Fig. 6**  $\chi^2$  contours are drawn in luminosity - lower limit on the Mixing angle plane for unpolarised ( $-80\%$  polarised) corresponding to the contribution from charged current process in the FCC-eh setup with  $\delta_{sys} = 5\%$ .

Similarly in Fig. 5 we have displayed the one  $\sigma$  (in red), two  $\sigma$  (in green) and three  $\sigma$  (in blue) exclusion contours in  $\tilde{a} - \tilde{b}$  plane for the FCC-eh set up with electron and proton beam energy of 150 GeV and 50 TeV, respectively. The first two figures on the upper panel are drawn from the contributions of CC process where the left panel and right panel correspond to the unpolarised and  $-80\%$  polarised electron beams respectively with zero systematic error and an integrated luminosity  $\mathcal{L} = 10 \text{ ab}^{-1}$ . The lower panel of two figures depict the contours drawn from the differential distributions of the sub-dominant NC process corresponding to the unpolarised and  $-80\%$  polarised electron beams, respectively with zero systematic error and an enhanced integrated luminosity  $\mathcal{L} = 10 \text{ ab}^{-1}$ . In all the four panels we draw the black colour contour for  $\tilde{a}^2 + \tilde{b}^2 = 1$  to extract the lower limits of mixing angles that can be measured in the proposed FCC-eh collider at 68%, 95% and 99.7% C.L. respectively. These lower limits on mixing angles at the 1  $\sigma$ , 2  $\sigma$  and 3  $\sigma$  C.L. are given in Table 2 for two choices of integrated luminosities  $\mathcal{L} = 1$  and  $10 \text{ ab}^{-1}$  and three representative values of systematic errors (0%, 5% and 10%) corresponding to each luminosity choice.<sup>1</sup>

Finally we analyse  $\chi^2$  as a function of the luminosity and the lower limit on the mixing angle upto which the proposed FCC-eh collider can be sensitive at a chose value of C.L. Fig. 6 display the 68% (red and blue) and 95% (green and black) C.L. contours in luminosity - lower limit of the

<sup>1</sup>Due to the small cross section and computational limitations in case of Fig. 4, we restrain ourselves to provide the 3  $\sigma$  contour. For similar reasons, we have not provided the 3  $\sigma$  limits in Table 2 for unpolarised charged current process.

Process	Pol.	CL	LHeC with $L = 1 \text{ ab}^{-1}$			FCC-eh with $L = 1 \text{ ab}^{-1}$			FCC-eh with $L = 10 \text{ ab}^{-1}$		
			$\delta_{\text{sys}}$			$\delta_{\text{sys}}$			$\delta_{\text{sys}}$		
			0%	5%	10%	0%	5%	10%	0%	5%	10%
CC	0%	$1\sigma$	16.8°	16.9°	17.1°	8.3°	8.5°	9.0°	2.6°	3.1°	4.3°
		$2\sigma$	32.6°	32.8°	33.4°	17.0°	17.5°	18.7°	5.1°	6.1°	8.6°
		$3\sigma$	—	—	—	23.7°	24.4°	26.4°	6.7°	8.1°	11.4°
	−80%	$1\sigma$	11.5°	11.6°	12.0°	6.8°	7.0°	7.9°	2.1°	2.9°	4.4°
		$2\sigma$	24.5°	24.9°	26.0°	13.7°	14.3°	16.0°	4.2°	5.6°	8.8°
		$3\sigma$	36.6°	37.4°	39.9°	18.6°	19.5°	22.1°	5.5°	7.5°	11.7°
NC	0%	$1\sigma$	—	—	—	—	—	—	5.8°	6.1°	7.0°
		$2\sigma$	—	—	—	—	—	—	11.6°	12.3°	14.1°
		$3\sigma$	—	—	—	—	—	—	15.7°	16.7°	19.3°
	−80%	$1\sigma$	—	—	—	—	—	—	5.6°	5.9°	6.8°
		$2\sigma$	—	—	—	—	—	—	11.0°	11.6°	13.4°
		$3\sigma$	—	—	—	—	—	—	14.6°	15.5°	17.9°

**Table 2** Figure of merit displaying the lower limits on the mixing angle  $\phi_\tau$  upto which the proposed LHeC and FCC-eh colliders can probe with 68%, 95% and 99.7% C.L. based on the  $\chi^2$  analysis for CC and NC processes. The sensitivities are computed using differential bin-width  $\Delta\alpha_{CP} = 30^\circ$  corresponding to three choices of the systematic errors for a given integrated luminosity.

mixing angle plane with  $\delta_{\text{sys}}$  5%, for the dominant charge current contribution at FCC-eh set up corresponding to unpolarised and −80% polarised 150 GeV electron beams, respectively.

#### 4.1 Contamination due to $Z/\gamma^*$ background

We’ve discussed about the results at the parton level so far, and computed the sensitivity of the  $CP$  sensitive observable,  $\alpha_{CP}$ , to constrain the  $CP$  admixture of the spin-0 mediator decaying to pair of  $\tau$  leptons. However, if we add the potential backgrounds with realistic effects owing to showering, hadronization, and detector architecture, these results are likely to be altered. We’ll go through each of them briefly in this sub-section.

In the  $CP$  study of scalar boson at  $e^-p$  collider, we strategize to minimise contamination from the dominant background ( $\sim$  six times larger than signal) where  $\tau$ -leptons are produced from  $Z$ -boson and/or  $\gamma^*$  decay in addition to the aforementioned background of the SM Higgs boson  $0^+$  state decaying to di-tau. Background contamination from the other potential sources contributing to formation of prompt soft pions is however, negligible for  $p_{T\pi^{\pm,0}} \geq 20 \text{ GeV}$ .<sup>2</sup>

In order to compute the efficiency with which we can discriminate and minimize the  $Z^0/\gamma^*$  background from the decay products of spin-0 state, we employ a deep neural network (DNN) learning algorithm consisting of one input layer with 20 nodes and one output layer with activation function sigmoid. In addition, we have three hidden layers with nodes corresponding to each layers are 200, 200 and 20 respectively. The activation function for the input and the hidden layers are chosen to be `relu`. We then optimized

<sup>2</sup>In addition, this cut is also very important in controlling the soft charged tracks inside the  $\tau$ -jet radius which may affect the shape of the  $\alpha_{CP}$  observable.

the DNN where the learning rate,  $\beta_1$ ,  $\beta_2$  and  $\varepsilon$  were set to their default values as 0.0005, 0.9, 0.999,  $1e^{-08}$  respectively. We have chosen Adam as the optimizer and binary crossentropy as the loss function. We split the data set for training and testing as 70% and 30% respectively with 30 epochs and batch size of 50.

The network’s input kinematic variables are combination of both the low level and the high level observables. The low-level inputs are the four momenta of the final state charged and neutral pions produced from the decays of  $\tau$ -leptons, whereas the high-level input observables are  $\Delta\phi$ ,  $\Delta R = \sqrt{(\Delta\eta)^2 + (\Delta\phi)^2}$  and invariant mass of reconstructed  $\rho^\pm$  from the observed four pions, reconstructed  $\tau$  pairs and missing transverse momenta. Since both  $m_\tau/m_Z$  and  $m_\tau/m_{H^0}$  are  $\ll 1$ , we assume that  $\tau$ ’s are highly boosted and therefore, we have adopted the collinear approximation to reconstruct the invisible neutrino momenta and then reconstruct the  $\tau$ -pair invariant mass. Now, among all the input variables to the network, we removed the ones that are highly correlated with others. Here, we utilise Pearson correlation to compute the correlation among the input variables. Following that, the network is fed with a total of 23 kinematic observables. With this, we can separate the signal from the background with an accuracy of 83%. All of these findings are for the parton level sample, and the details may be seen in the Appendix below.

We find that the DNN enhances the sensitivity of the  $CP$  phase determination in the  $\chi^2$  analysis and further lowers the one sigma limit to  $16.0^\circ$  for polarized LHeC with luminosity of  $1 \text{ ab}^{-1}$ . The results for other cases are also similarly affected. In the following we will discuss the effects of the detector simulation on these sensitivities.

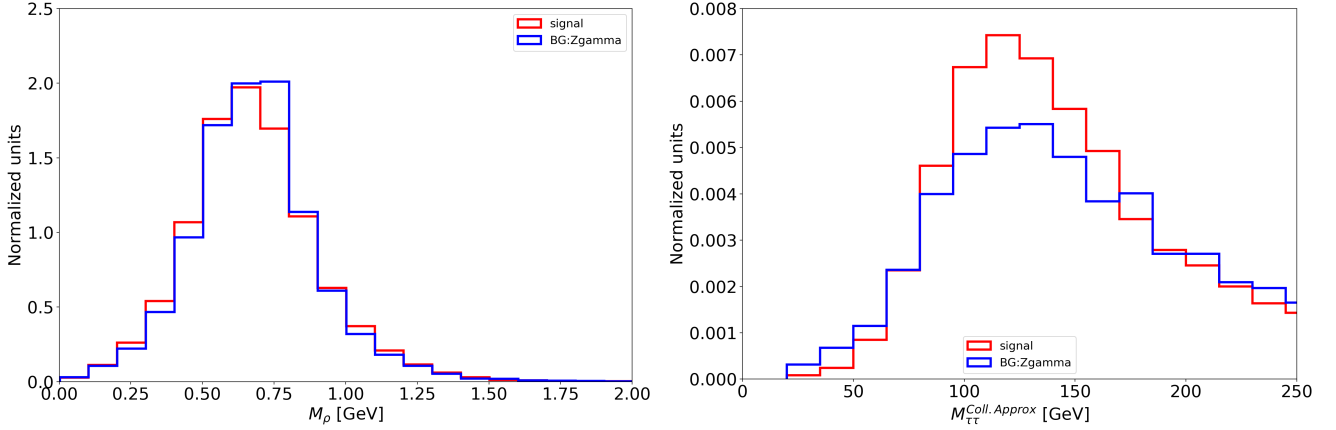


**Fig. 7** Left panel displays the distribution of the rho mass computed from the charged pions and the neutral pions. In the right panel we show the reconstructed  $\tau$  pair invariant mass using the collinear approximation. Clearly the collinear approximation works well in getting the Higgs boson mass at the correct value.

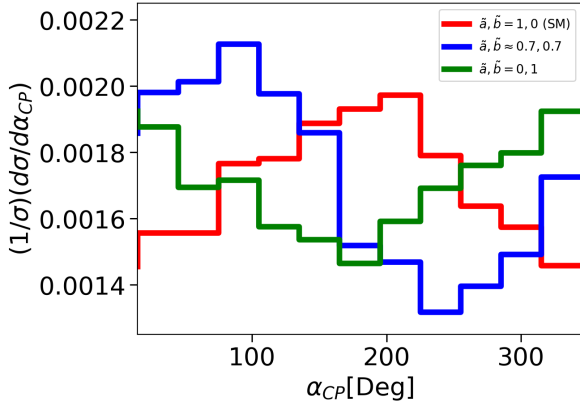


**Fig. 8** Here we present the distribution of the  $\alpha_{CP}$  after the detector simulation. The red, blue and green distributions represent the  $CP$ -phase zero,  $\pi/4$  and  $\pi/2$  respectively. Evidently the  $\alpha_{CP}$  observable is very important in constraining the  $CP$ -phase.

#### 4.2 Detector Simulation

We have done showering and hadronization using Pythia8 [79]. Since Pythia8 is still new to handle the  $e^-p$  collider environment we have adjusted few settings in a standalone Pythia8 code<sup>3</sup> to enable the showering and hadronization. The detector simulation is performed using Delphes3 [80]. As the LHeC and FCC-eh are asymmetric colliders the  $\eta$  ranges of the final state particles are very different from a symmetric collider like LHC, so we have modified the detector card accordingly to take care of that issue [11]. Additionally, we also have modified the efficiencies and isolation criteria of different objects as per the technical design report of these colliders [6]. The jet construction are done using

<sup>3</sup>We had a private communication with the Pythia8 authors and following the suggestion we have switched off the QED radiation from the lepton and also switched off the the input matching of the LesHouches input obtained from Madgraph5.

Fastjet [81] which utilize anti- $k_T$  algorithm with radius  $R = 0.5$  and  $p_T > 20$  GeV.

The events are selected with at least two  $\tau$  jets with  $p_T > 20$  GeV and we have not put any cuts on  $\eta$  because of the asymmetric nature of the collider. Once we have get the  $\tau$  jets we get the  $\tau$  constituents from which tracks gives the charged pions and the tower corresponds to the neutral pions. Since in most of the cases there are many charged tracks and also many entries in the tower, so one should make sure that the right combination of the charged track and tower should be selected such that the invariant mass is close to the  $\rho$  meson mass (770 MeV). In Fig. 7 left panel we display the reconstructed  $\rho$  meson mass obtained from the charged and neutral pions four momenta that we get from the track and tower.

With the correct combination of charged and neutral pions, we can reconstruct the neutrinos to obtain the  $\tau$  lepton pair invariant mass. For the hadronic decays of the  $\tau$ 's, two neutrinos are present in each event, which are boosted and are collinear with respect to their parents. The collinear approximation, however, assumes that there is no other source of the missing transverse energy other than neutrinos. But in the charged current mechanism we studied here, the forward neutrino provides an additional source of missing transverse energy, causing the invariant mass to have a large tail.

In the right panel of Fig. 7 we display the  $\tau$  pair invariant mass which is peaking at the Higgs boson mass. We observe that the forward neutrino contribution to the missing energy from the spin-1 background is more prominent than the signal.

To maximise the signal to background ratio, we use the same deep learning network structure and train with the same observable as in the parton-level analysis, resulting in a 73% accuracy. For both testing and training samples, the area under the curve (AUC) of the receiver operating characteristic (ROC) curve is 80%. The distributions of the  $\alpha_{CP}$  are



shown in Fig. 8 with red, blue, and green colour histograms, which correspond to the  $CP$  phases zero,  $\pi/4$ , and  $\pi/2$ , respectively. The distributions for the FCC-eh polarised collider are shown here.

Using the  $\chi^2$  analysis that we described before, we get  $23.32^\circ$  at  $1\sigma$  for  $3 \text{ ab}^{-1}$  luminosity and  $46.0^\circ$  at  $2\sigma$  for this  $CP$  sensitive observable. We can further improve and constrain the  $CP$ -phase to  $11.4^\circ$  at  $1\sigma$  and  $24.0^\circ$  at  $2\sigma$  for polarized electron beam at FCC-eh.

## 5 Summary and Conclusion

In this article we explore the  $CP$  mixing probability of  $h$  through its decay to  $\tau^+\tau^-$  in the future  $e^-p$  collider, where  $h$  is singly produced in the charged and neutral current modes through  $W^+W^-$  and  $ZZ$ -fusion, respectively. To explore the  $CP$  nature through the  $h\tau\bar{\tau}$  coupling, we consider the  $\tau^\pm \rightarrow \pi^\pm + \pi^0 + \bar{\nu}_\tau/\nu_\tau$  decay modes as this channel has largest branching fraction of about 25%. We have deployed an interesting observable,  $\alpha_{CP}$ , which does not require reconstruction of  $\tau^\pm$  to scrutinise the  $CP$  sensitivity of  $h\tau\bar{\tau}$  coupling. With this observable we employed  $\chi^2$  between the SM expectation and new physics to estimate the sensitivity.

The sensitivity that is obtained from this analysis with charged current at the LHeC with  $\mathcal{L} = 1 \text{ ab}^{-1}$  is  $17^\circ$  ( $12^\circ$ ) for unpolarised (polarised) electron beam at 68% C.L. when uncertainty is 10%. The sensitivity at 95% C.L. is  $33^\circ$  ( $26^\circ$ ) for unpolarised (polarised) electron beam. Expectedly, the best limit is obtained from the FCC-eh with charged current process at  $\mathcal{L} = 10 \text{ ab}^{-1}$ ,  $4^\circ$  at 68% C.L. while  $9^\circ$  at 95% C.L. with 10% uncertainty. Similarly, the sensitivity for FCC-eh at  $1 \text{ ab}^{-1}$  is  $9.0^\circ$  ( $8.0^\circ$ ) and  $18.7^\circ$  ( $16.0^\circ$ ) at 68% and 95% C.L. respectively for unpolarised (polarised) electron beam respectively. The limit for the neutral current is very weak for LHeC setup and even for FCC-eh and hence the limits are not shown here. Hence, the sensitivity for neutral current is shown for FCC-eh with  $\mathcal{L} = 10 \text{ ab}^{-1}$ . This limit is  $7.0^\circ$  and  $14.0^\circ$  at 68% and 95% C.L. respectively. Here also we have considered 10% uncertainty in the computation. Hence, it is evident from this analysis that the  $CP$  phase of  $h\tau\bar{\tau}$  coupling can be measured quite efficiently in a futuristic  $e^-p$  collider and the sensitivity might be comparative, if not better, compared to the limit obtained from LHC. Although at the LHC the production cross section is higher than what we can expect at a  $e^-p$  collider, in the respect of backgrounds  $e^-p$  machine has low backgrounds making the limits obtained from them are comparable with LHC.

Considering the effects of background(s) and smearing at the detector-level the sensitivities of  $CP$ -phase observable is affected and studied. With the  $\chi^2$  analysis using the  $CP$ -phase observable, the  $CP$  admixture of the  $h\tau\bar{\tau}$  coupling is constrained to  $23.32^\circ$  ( $46.0^\circ$ ) at 1 (2)  $\sigma$  for  $3 \text{ ab}^{-1}$  luminosity in the case of FCC-eh where  $E_e = 150 \text{ GeV}$  and

$E_p = 50 \text{ TeV}$ . However, at  $\mathcal{L} = 10 \text{ ab}^{-1}$  it is  $11.4^\circ$  ( $24.0^\circ$ ) at 1 (2)  $\sigma$ .

It is important to mention that in this study  $h\tau\bar{\tau}$  is taken to be the only  $CP$ -violating coupling, all other couplings used in this work are the SM couplings. Though the  $CP$  nature of  $hWW/hZZ$  couplings has been studied in literature [10, 11] and one can also perform a global analysis considering the  $CP$  structure at production as well as at the decay vertex. The  $CP$  nature of  $h$  can also be probed through its production in association with top-quarks [12] and there one can simultaneously account the  $CP$  admixture at  $h$ -decay vertex via  $h \rightarrow \tau^+\tau^-$ . This channel also open a space to probe simultaneous measurement of  $hWW$ ,  $Wtb$ ,  $ht\bar{t}$  and  $h\tau\bar{\tau}$  couplings and we keep these possibilities for future studies.

## Acknowledgements

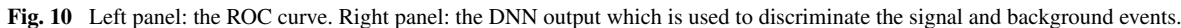
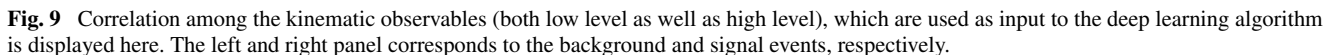
The work of SD, AG and AKS was partially supported by the SERB, Govt. of India under CRG/2018/004889. We thank Satyaki Bhattacharya, Kai Ma and Ilkka Helenius for useful discussion.

## Appendix

Here we discuss about the deep learning algorithm that we employed in this analysis. The basic kinematic observables like transverse momenta ( $p_T$ ), pseudo rapidity ( $\eta$ ), azimuthal angle ( $\phi$ ) and energy ( $E$ ) of each charged and neutral pions are referred as low level variables. The high level variables are the ones constructed from the low level variables such as  $\Delta\phi_{ij}$ ,  $\Delta R_{ij}$ , invariant mass ( $M_{ij}$ ) etc. Here  $i, j = \pi^-, \pi^+, \pi^0, \pi^0$  with  $0^\pm$  in the superscript refers to the neutral pions produced from  $\tau^\pm$ .

In Fig. 9 we show the correlation among the kinematic observables, input to the deep learning algorithm. The left (right) panel corresponds to background (signal) events. There few other kinematic variables which can be there but we have removed them from the list because of the high correlation with other existing variables. Both for the signal and the background events the correlation among different variables are more or less similar.

We also show here the ROC curve and the deep learning algorithm output to discriminate the signal and background in Fig. 10. This is done at the parton level with  $CP$  phase 0 of Higgs to  $\tau$  pair sample as the signal. We have done the same exercise for the other  $CP$  phase values like  $\pi/4$  and  $\pi/2$  and found that the result remains the same. This is essentially because the kinematic observables are more or less insensitive to the  $CP$  phase of the Higgs to  $\tau$  pair samples. The right panel describes the deep learning output for the signal and background events on the testing sample with which the algorithm has not been trained. It is also evident from



## References

- this that the deep learning algorithm learned the differences between the signal and background kinematics and successfully separated them. At the detector level we also observed the similar separation of signal and background events from the DNN algorithm used in this work.
- ## References
1. G. Aad *et al.* [ATLAS], Phys. Lett. B **726**, 120-144 (2013) [arXiv:1307.1432 [hep-ex]].
  2. G. Aad *et al.* [ATLAS], Phys. Lett. B **716** (2012), 1-29 [arXiv:1207.7214 [hep-ex]].
  3. S. Chatrchyan *et al.* [CMS], Phys. Lett. B **716** (2012), 30-61 [arXiv:1207.7235 [hep-ex]].
  4. G. Aad *et al.* [ATLAS], Phys. Lett. B **726** (2013), 88-119 [erratum: Phys. Lett. B **734** (2014), 406-406] [arXiv:1307.1427 [hep-ex]].
  5. [CMS], CMS-PAS-HIG-19-009.
  6. LHeC Study Group Collaboration, J. Phys. G **39**, 075001 (2012). <http://lhec.web.cern.ch/>
  7. O. Bruening and M. Klein, Mod. Phys. Lett. A **28**, 1330011 (2013).
  8. P. Agostini *et al.* [LHeC and FCC-he Study Group], [arXiv:2007.14491 [hep-ex]].
  9. A. Abada *et al.* [FCC], Eur. Phys. J. C **79**, no.6, 474 (2019)
  10. S. S. Biswal, R. M. Godbole, B. Mellado and S. Raychaudhuri, Phys. Rev. Lett. **109**, 261801 (2012).
  11. M. Kumar, X. Ruan, R. Islam, A. S. Cornell, M. Klein, U. Klein and B. Mellado, Phys. Lett. B **764**, 247-253 (2017) [arXiv:1509.04016 [hep-ph]].
  12. B. Coleppa, M. Kumar, S. Kumar and B. Mellado, Phys. Lett. B **770**, 335-341 (2017) [arXiv:1702.03426 [hep-ph]].
  13. S. F. Ge, G. Li, P. Pasquini and M. J. Ramsey-Musolf, Phys. Rev. D **103** (2021) no.9, 095027 [arXiv:2012.13922 [hep-ph]].
  14. P. Basler, M. Mühlleitner and J. Wittbrodt, JHEP **03** (2018), 061 [arXiv:1711.04097 [hep-ph]].

15. F. U. Bernlochner, C. Englert, C. Hays, K. Lo-hwasser, H. Mildner, A. Pilkington, D. D. Price and M. Spannowsky, *Phys. Lett. B* **790** (2019), 372-379 [arXiv:1808.06577 [hep-ph]].
16. J. Shu and Y. Zhang, *Phys. Rev. Lett.* **111** (2013) no.9, 091801 [arXiv:1304.0773 [hep-ph]].
17. C. W. Chiang, K. Fuyuto and E. Senaha, *Phys. Lett. B* **762**, 315-320 (2016) [arXiv:1607.07316 [hep-ph]].
18. S. Chatrchyan *et al.* [CMS], *Phys. Rev. Lett.* **110**, no.8, 081803 (2013) [arXiv:1212.6639 [hep-ex]].
19. S. Chatrchyan *et al.* [CMS], *Phys. Rev. D* **89**, no.9, 092007 (2014) [arXiv:1312.5353 [hep-ex]].
20. V. Khachatryan *et al.* [CMS], *Phys. Rev. D* **92**, no.1, 012004 (2015) [arXiv:1411.3441 [hep-ex]].
21. V. Khachatryan *et al.* [CMS], *Phys. Lett. B* **759**, 672-696 (2016) [arXiv:1602.04305 [hep-ex]].
22. Y. Chen, A. Falkowski, I. Low and R. Vega-Morales, *Phys. Rev. D* **90** (2014) no.11, 113006 [arXiv:1405.6723 [hep-ph]].
23. Y. Chen, R. Harnik and R. Vega-Morales, *Phys. Rev. Lett.* **113** (2014) no.19, 191801 [arXiv:1404.1336 [hep-ph]].
24. F. Bishara, Y. Grossman, R. Harnik, D. J. Robinson, J. Shu and J. Zupan, *JHEP* **04** (2014), 084 [arXiv:1312.2955 [hep-ph]].
25. A. Y. Korchin and V. A. Kovalchuk, *Phys. Rev. D* **88** (2013) no.3, 036009 [arXiv:1303.0365 [hep-ph]].
26. R. Harnik, A. Martin, T. Okui, R. Primulando and F. Yu, *Phys. Rev. D* **88** (2013) no.7, 076009 [arXiv:1308.1094 [hep-ph]].
27. M. J. Dolan, P. Harris, M. Jankowiak and M. Spannowsky, *Phys. Rev. D* **90** (2014), 073008 [arXiv:1406.3322 [hep-ph]].
28. D. L. Rainwater, D. Zeppenfeld and K. Hagiwara, *Phys. Rev. D* **59**, 014037 (1998) [arXiv:hep-ph/9808468 [hep-ph]].
29. J. R. Dell'Aquila and C. A. Nelson, *Phys. Rev. D* **33** (1986), 93
30. J. R. Dell'Aquila and C. A. Nelson, *Nucl. Phys. B* **320** (1989), 61-85
31. W. Bernreuther and A. Brandenburg, *Phys. Lett. B* **314** (1993), 104-111
32. W. Bernreuther and A. Brandenburg, *Phys. Rev. D* **49** (1994), 4481-4492 [arXiv:hep-ph/9312210 [hep-ph]].
33. A. Soni and R. M. Xu, *Phys. Rev. D* **48** (1993), 5259-5263 [arXiv:hep-ph/9301225 [hep-ph]].
34. A. Skjold and P. Osland, *Phys. Lett. B* **329** (1994), 305-311 [arXiv:hep-ph/9402358 [hep-ph]].
35. B. Grzadkowski and J. F. Gunion, *Phys. Lett. B* **350** (1995), 218-224 [arXiv:hep-ph/9501339 [hep-ph]].
36. B. Grzadkowski, J. F. Gunion and J. Kalinowski, *Phys. Rev. D* **60** (1999), 075011 [arXiv:hep-ph/9902308 [hep-ph]].
37. K. Hagiwara, S. Ishihara, J. Kamoshita and B. A. Kniehl, *Eur. Phys. J. C* **14** (2000), 457-468 [arXiv:hep-ph/0002043 [hep-ph]].
38. T. Han and J. Jiang, *Phys. Rev. D* **63** (2001), 096007 [arXiv:hep-ph/0011271 [hep-ph]].
39. T. Plehn, D. L. Rainwater and D. Zeppenfeld, *Phys. Rev. Lett.* **88** (2002), 051801 [arXiv:hep-ph/0105325 [hep-ph]].
40. S. Y. Choi, D. J. Miller, M. M. Muhlleitner and P. M. Zerwas, *Phys. Lett. B* **553** (2003), 61-71 [arXiv:hep-ph/0210077 [hep-ph]].
41. G. R. Bower, T. Pierzchala, Z. Was and M. Worek, *Phys. Lett. B* **543** (2002), 227-234 [arXiv:hep-ph/0204292 [hep-ph]].
42. K. Desch, Z. Was and M. Worek, *Eur. Phys. J. C* **29** (2003), 491-496 [arXiv:hep-ph/0302046 [hep-ph]].
43. E. Asakawa and K. Hagiwara, *Eur. Phys. J. C* **31** (2003), 351-364 [arXiv:hep-ph/0305323 [hep-ph]].
44. K. Desch, A. Imhof, Z. Was and M. Worek, *Phys. Lett. B* **579** (2004), 157-164 [arXiv:hep-ph/0307331 [hep-ph]].
45. R. M. Godbole, S. Kraml, M. Krawczyk, D. J. Miller, P. Niezurawski and A. F. Zarnecki, [arXiv:hep-ph/0404024 [hep-ph]].
46. A. Rouge, *Phys. Lett. B* **619** (2005), 43-49 [arXiv:hep-ex/0505014 [hep-ex]].
47. S. S. Biswal, R. M. Godbole, R. K. Singh and D. Choudhury, *Phys. Rev. D* **73** (2006), 035001 [erratum: *Phys. Rev. D* **74** (2006), 039904] [arXiv:hep-ph/0509070 [hep-ph]].
48. R. M. Godbole, D. J. Miller and M. M. Muhlleitner, *JHEP* **12** (2007), 031 [arXiv:0708.0458 [hep-ph]].
49. P. S. Bhupal Dev, A. Djouadi, R. M. Godbole, M. M. Muhlleitner and S. D. Rindani, *Phys. Rev. Lett.* **100** (2008), 051801 [arXiv:0707.2878 [hep-ph]].
50. S. Berge, W. Bernreuther and J. Ziethe, *Phys. Rev. Lett.* **100** (2008), 171605 [arXiv:0801.2297 [hep-ph]].
51. A. De Rujula, J. Lykken, M. Pierini, C. Rogan and M. Spiropulu, *Phys. Rev. D* **82** (2010), 013003 [arXiv:1001.5300 [hep-ph]].
52. N. D. Christensen, T. Han and Y. Li, *Phys. Lett. B* **693** (2010), 28-35 [arXiv:1005.5393 [hep-ph]].
53. S. Berge, W. Bernreuther, B. Niepelt and H. Spiesberger, *Phys. Rev. D* **84** (2011), 116003 [arXiv:1108.0670 [hep-ph]].
54. R. M. Godbole, C. Hangst, M. Muhlleitner, S. D. Rindani and P. Sharma, *Eur. Phys. J. C* **71** (2011), 1681 [arXiv:1103.5404 [hep-ph]].
55. S. Berge, W. Bernreuther and H. Spiesberger, *Phys. Lett. B* **727** (2013), 488-495 [arXiv:1308.2674 [hep-ph]].
56. A. Hayreter and G. Valencia, *JHEP* **07** (2015), 174 [arXiv:1505.02176 [hep-ph]].

57. T. Han, S. Mukhopadhyay, B. Mukhopadhyaya and Y. Wu, JHEP **05** (2017), 128 [arXiv:1612.00413 [hep-ph]].
58. A. K. Swain, [arXiv:2008.11127 [hep-ph]].
59. J. R. Ellis, J. S. Lee and A. Pilaftsis, Phys. Rev. D **72** (2005), 095006 [arXiv:hep-ph/0507046 [hep-ph]].
60. A. Bhardwaj, P. Konar, P. Sharma and A. K. Swain, J. Phys. G **46** (2019) no.10, 105001 [arXiv:1612.01417 [hep-ph]].
61. S. Berge and W. Bernreuther, Phys. Lett. B **671** (2009), 470-476 [arXiv:0812.1910 [hep-ph]].
62. K. Hagiwara, K. Ma and S. Mori, Phys. Rev. Lett. **118** (2017) no.17, 171802 [arXiv:1609.00943 [hep-ph]].
63. S. Berge, W. Bernreuther and S. Kirchner, Eur. Phys. J. C **74** (2014) no.11, 3164 [arXiv:1408.0798 [hep-ph]].
64. [CMS], CMS-PAS-HIG-20-006.
65. K. Hagiwara, T. Li, K. Mawatari and J. Nakamura, Eur. Phys. J. C **73**, 2489 (2013) [arXiv:1212.6247 [hep-ph]].
66. S. Jadach, J. H. Kuhn and Z. Was, Comput. Phys. Commun. **64** (1990), 275-299 doi:10.1016/0010-4655(91)90038-M
67. J. H. Kuhn and A. Santamaria, Z. Phys. C **48** (1990), 445-452 doi:10.1007/BF01572024
68. A. Alloul, N. D. Christensen, C. Degrande, C. Duhr and B. Fuks, Comput. Phys. Commun. **185** (2014), 2250-2300 [arXiv:1310.1921 [hep-ph]].
69. J. Alwall, R. Frederix, S. Frixione, V. Hirschi, F. Maltoni, O. Mattelaer, H. S. Shao, T. Stelzer, P. Torrielli and M. Zaro, JHEP **07** (2014), 079 [arXiv:1405.0301 [hep-ph]].
70. R. D. Ball, V. Bertone, S. Carrazza, C. S. Deans, L. Del Debbio, S. Forte, A. Guffanti, N. P. Hartland, J. I. Latorre and J. Rojo, *et al.* Nucl. Phys. B **867** (2013), 244-289 [arXiv:1207.1303 [hep-ph]].
71. P. Konar and A. K. Swain, Phys. Rev. D **93** (2016) no.1, 015021 [arXiv:1509.00298 [hep-ph]].
72. P. Konar and A. K. Swain, Phys. Lett. B **757** (2016), 211-215 [arXiv:1602.00552 [hep-ph]].
73. A. K. Swain and P. Konar, JHEP **03** (2015), 142 [arXiv:1412.6624 [hep-ph]].
74. S. Maruyama, [arXiv:1512.04842 [hep-ex]].
75. B. Gripaios, K. Nagao, M. Nojiri, K. Sakurai and B. Webber, JHEP **03** (2013), 106 [arXiv:1210.1938 [hep-ph]].
76. L. G. Xia, Chin. Phys. C **40** (2016) no.11, 113003 [arXiv:1601.02454 [hep-ex]].
77. A. Elagin, P. Murat, A. Pranko and A. Safonov, Nucl. Instrum. Meth. A **654** (2011), 481-489 [arXiv:1012.4686 [hep-ex]].
78. R. K. Ellis, I. Hinchliffe, M. Soldate and J. J. van der Bij, Nucl. Phys. B **297** (1988), 221-243
79. T. Sjostrand, S. Mrenna and P. Z. Skands, JHEP **05**, 026 (2006) doi:10.1088/1126-6708/2006/05/026 [arXiv:hep-ph/0603175 [hep-ph]].
80. J. de Favereau *et al.* [DELPHES 3], JHEP **02**, 057 (2014) doi:10.1007/JHEP02(2014)057 [arXiv:1307.6346 [hep-ex]].
81. M. Cacciari, G. P. Salam and G. Soyez, Eur. Phys. J. C **72**, 1896 (2012) doi:10.1140/epjc/s10052-012-1896-2 [arXiv:1111.6097 [hep-ph]].